International Journal of Non-Linear Mechanics 118 (2020) 103241

Contents lists available at ScienceDirect

International Journal of Non-Linear Mechanics

journal homepage: www.elsevier.com/locate/nlm

Strain-induced phase transformation in poly(lactic acid) across the glass transition: Constitutive model and identification

Hanen Mahjoubi [a], Fahmi Zaïri [b,*], Zoubeir Tourki [a]

[a] Sousse University, Sousse Mechanical Laboratory, 264 Sousse, Tunisia
[b] Lille University, Civil Engineering and geo-Environmental Laboratory (EA 4515 LGCgE), 59000 Lille, France

ARTICLE INFO

Keywords:
Poly(lactic acid)
Strain-induced phase transformation
Mesomorphic/crystalline phases
Elastic–viscoplastic–viscohyperelastic

ABSTRACT

Poly(lactic acid) (PLA) is one of the most popular environmental-friendly materials derived from renewable agricultural resources. One of the most important features of this biomaterial is its ability to develop a phase transformation under straining. Two strain-induced phases can potentially form, namely mesomorphic and crystalline, whose respective occurrence is highly temperature and rate-dependent. The aim of the present contribution is to provide a quantitative predictive modeling of this phenomenon. A large-strain constitutive model is proposed to describe the strain-induced phase transformation in PLA along with the stress–strain behavior over a wide range of straining temperatures across the glass transition involving glassy to rubbery response. The material response is decomposed into two physically distinct sources, an elastic–viscoplastic intermolecular resistance to deformation and a viscohyperelastic molecular network resistance to stretching and chain orientation. The effective contribution of the amorphous, mesomorphic and crystalline phases to the intermolecular resistance is treated in a composite framework considering a three-phase representation of the microstructure. Using experimental data of an initially amorphous PLA extracted from the literature, the dual-phase transformation kinetics is designed and the properties of each phase are isolated. The proposed model is found to successfully capture the important features of the experimental observations in terms of strain-induced phase transformation and mechanical response over a large strain range, a wide range of temperatures and two strain rates. The model is then used to discuss some important aspects of the connection between the phenomenon of phase changes and the material response.

1. Introduction

Development of biodegradable polymers represents the largest and fastest growing area for ecological purpose. Nowadays, there is a strong demand to find engineering polymers produced from renewable bio-based raw materials that can be substitutes to traditional petroleum-based polymers. Among those bio-polymers, poly(lactic acid) (PLA) has attracted a lot of attention in the recent literature [1–16]. This biodegradable thermoplastic polyester is one of the most popular environmental-friendly materials derived from renewable agricultural resources, e.g. corn-starch. The commercial introduction of bio-based PLA begins in 2003 and has open the way for many applications in the packaging and biomedical industries, particularly for its good properties close to traditional petroleum-based polymers, its transparency, its compostability, its biocompatibility and its bioresorbability [4,15,16]. An accurate knowledge of the PLA response in connection to the microstructure is of prime importance to improve performance.

A phenomenon of phase changes occurs during the straining of PLA. Several studies showed that a part of the amorphous phase is transformed into two substructures, namely mesomorphic and crystalline phases [3,7–14]. Mulligan and Cakmak [3] observed, during the straining of PLA, this new structure somewhat different of the amorphous phase and possessing a "nematic-like" order. The occurrence of the mesomorphic phase in PLA, which has an intermediate ordering between amorphous and crystal, is attributed to a limited molecular mobility and relatively high entanglement densities preventing the lateral arrangement of the molecular chains for crystallization. This strain-induced imperfect order is thermally stable in PLA, surviving from melting below the glass transition temperature T_g and at a short temperature range above T_g [7–9,11]. An increase of the thermal stability with the PLA straining is reported. Moreover, both temperature and strain rate influence in a significant manner the occurrence of the two strain-induced phases [7,8,14]. Indeed, the strain-induced orientation and the thermal-induced chain relaxation are competitive processes mainly governed by the straining temperature and the strain rate. A diagram in Fig. 1 summarizes their influence by plotting the straining temperature and the strain rate in two axes. At high straining temperature, although the rate of chain relaxation is important, the

* Corresponding author.
E-mail address: fahmi.zairi@polytech-lille.fr (F. Zaïri).

https://doi.org/10.1016/j.ijnonlinmec.2019.103241
Received 27 July 2018; Received in revised form 27 June 2019; Accepted 6 August 2019
Available online 9 August 2019
0020-7462/

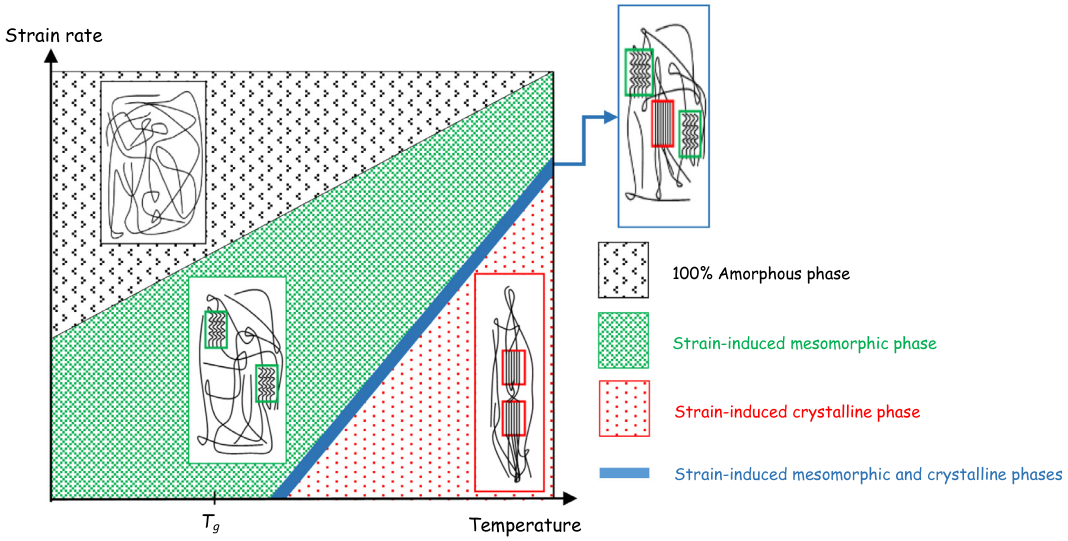

Fig. 1. Phase diagram of PLA; adapted from the experimental observations of Stoclet et al. [7,8].

crystallization occurs as long as the strain rate is low. With increasing the strain rate, the two strain-induced substructures may co-exist when the ratio between chain orientation and relaxation is the most favorable. If the strain rate is increased more, only the imperfect ordered mesomorphic form is developed in view of the fact that the chain relaxation rate is still high. When the strain rate is too fast, the chain relaxation rate is much slower than the chain orientation rate and neither the mesomorphic phase nor the crystalline phase occur.

The present work is aimed at modeling the strain-induced phase transformation in PLA along with the stress–strain behavior. Our goal is to propose a unified large-strain constitutive model valid over a wide range of straining temperatures across the glass transition. PLA presents a wide range of mechanical behaviors, which, in addition to be highly nonlinear, is highly temperature and rate-dependent. Below the transition temperature, the response is elastic–viscoplastic at small/moderate strains and progressively viscohyperelastic if large strains can be sustained by the material. When the straining temperature is higher than the glass transition, the viscohyperelasticity dominates. Various constitutive models have been developed to describe the large deformation of polymers exhibiting a yield event (Ref. [17–40] among many other references). Although the process of strain-induced crystallization has a depth impact on the response of crystallizable materials, a literature survey shows that there exist very few contributions dealing with their constitutive modeling. Some investigations focused on the first rubber used, namely natural rubber (NR), in which the first observation of the crystallization phenomenon was reported in 1925 by Katz [41]. The first theoretical bases for the strain-induced crystallization of this bio-material were provided by Flory in his early work [42] within the context of hyperelastic statistical mechanics. Recent research works proposed constitutive models to describe the strain-induced crystallization in NR [43–48] but restricted to the hyperelastic framework. The constitutive modeling of polymers near the glass transition, and thus involving potentially a yield event, requires to combine the (visco)hyperelastic framework to the elastic–viscoplastic framework. Most of works paid special attention to the most largely used strain-induced crystallizable petroleum-based polymer, namely poly(ethylene terephthalate) (PET) [17–23,25–27,31,36,37,39,49]. By contrast to NR in which the strain-induced crystallization is a recoverable mechanism [50], the phenomenon is unrecoverable in PET and in PLA. Although the mesomorphic phase is also observed in PET, it is not stable but acts as a precursor of the crystalline phase development during straining [51,52]. The modeling of the strain-induced phase changes in PLA is not referred in the literature and appears as a challenging task in view of the strong dependence on temperature and strain rate of the two newly developed substructures. The prediction of the mechanical response is a strong motivation for the better understanding of the benefits or prejudices of the mechanism of phase changes in PLA.

In this contribution, we present and discuss an internal state variable constitutive model to describe the progressive evolution of the mesomorphic/crystalline phases in PLA along with the elastic–viscoplastic–viscohyperelastic response over a large strain range involving, across the glass transition, thermoplastic-type to rubber-type mechanical response. The main objective is the consideration of the dual-phase transformation in the constitutive theory with the strong, and complex, influence of straining temperature and strain rate on the competitive process as illustrated in Fig. 1. The mechanical coupling between the three deformation modes in the elastic–viscoplastic intermolecular resistance, due to the presence of amorphous and mesomorphic/crystalline phases, is achieved within a composite framework. The latter is in turn coupled to a viscohyperelastic network resistance to molecular orientation and relaxation capturing the strain-hardening response. The material kinetics are designed using the experimental data of an initially amorphous PLA strained over a wide range of straining temperatures and two strain rates, in which the relationship between mesomorphic/crystalline phases and strain was established by means of X-ray diffraction technique by Stoclet et al. [7,8]. The parameters are determined according to a three-step strategy by (i) firstly designing the kinetics of the phase transformation, secondly (ii) calibrating the amorphous intermolecular properties using the elastic–viscoplastic region of the stress–strain curves and thirdly (iii) calibrating the mesomorphic/crystalline intermolecular properties and the network properties using the viscohyperelastic strain-hardening region of the stress–strain curves. The proposed model is used to discuss the connection between the phenomenon of phase changes, the physics of the deformation of the (amorphous, mesomorphic and crystalline) phases and the material response.

The outline of the present paper is as follows. Section 2 presents the main features of the constitutive theory. Section 3 provides comparisons of the model results and experimental data along with the methodology for the calibration of the model parameters and the phase transformation kinetics. Some concluding remarks are finally formulated in Section 4.

2. Model formulation

In this section, the theory for the finite deformation elastic-viscoplastic–viscohyperelastic modeling is summarized. The material

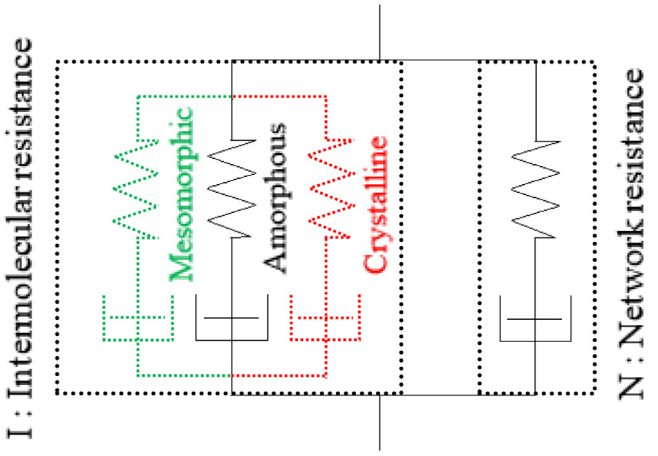

Fig. 2. Rheological representation of the model.

response is decomposed into two separate basic deformation mechanisms: One deals with the intermolecular interactions between neighboring polymer segments and the other accounts for the molecular network stretching and orientation process. The two mechanisms are supposed to participate to deformation via the Taylor assumption, i.e. parallelism. The intermolecular interactions are the origin of the elastic–viscoplastic response at small/moderate strains while the molecular network resistance is responsible for the viscohyperelastic dramatic hardening at large strains. Depending on strain rate and temperature, mesomorphic and/or crystalline phases develop in PLA which generates an increase in intermolecular barriers. Because the newly formed phases participate in the deformation, we assume that they act in parallel in the intermolecular resistance. The constitutive model is shown schematically in Fig. 2. The four branches are constituted by a spring in series with a viscous dashpot. In the following derivation, quantities devoted to the intermolecular and molecular network interactions will be referred with the subscript I and N, respectively.

The following notation is used throughout the text. Tensors and vectors are denoted by boldfaced letters while scalars and individual components of tensors are denoted by normal italicized letters. The superposed dot designates the time derivative.

2.1. Kinematics

The constitutive model is formulated within the large inelastic deformation kinematics framework which is briefly addressed in this subsection. The deformation gradient $\mathbf{F}$ is given by: $\mathbf{F} = \partial\mathbf{x}/\partial\mathbf{X}$ where $\mathbf{X}$ is the position of a material point in the reference configuration and $\mathbf{x}$ its position in the deformed configuration. It is multiplicatively decomposed into an elastic part $\mathbf{F}^e$ and an inelastic part $\mathbf{F}^p$ according to the approach proposed by Lee [53]: $\mathbf{F} = \mathbf{F}^e\mathbf{F}^p$. Since the model is based upon a parallel scheme, the deformation gradients in the four resistances $\mathbf{F}_{I\_a}$, $\mathbf{F}_{I\_m}$, $\mathbf{F}_{I\_c}$, $\mathbf{F}_N$ are equal to the imposed deformation gradient $\mathbf{F}$. The subscripts a, m and c refer to the amorphous, mesomorphic and crystalline phases, respectively.

Using the polar decomposition, the elastic part $\mathbf{F}^e_{I\_i}$ and the inelastic part $\mathbf{F}^p_{I\_i}$ of the intermolecular resistance may be expressed as the product of a stretch and a rotation:

$$\mathbf{F}^e_{I\_i} = \mathbf{R}^e_{I\_i}\mathbf{U}^e_{I\_i} = \mathbf{V}^e_{I\_i}\mathbf{R}^e_{I\_i} \quad \text{and} \quad \mathbf{F}^p_{I\_i} = \mathbf{R}^p_{I\_i}\mathbf{U}^p_{I\_i} = \mathbf{V}^p_{I\_i}\mathbf{R}^p_{I\_i} \tag{1}$$

in which the subscript i denotes the phase under consideration.

The elastic (network orientation) part $\mathbf{F}^e_N$ and the inelastic (flow) part $\mathbf{F}^p_N$ of the network resistance may be also decomposed using the polar decomposition:

$$\mathbf{F}^e_N = \mathbf{R}^e_N\mathbf{U}^e_N = \mathbf{V}^e_N\mathbf{R}^e_N \quad \text{and} \quad \mathbf{F}^p_N = \mathbf{R}^p_N\mathbf{U}^p_N = \mathbf{V}^p_N\mathbf{R}^p_N \tag{2}$$

The rate kinematics for the intermolecular and network resistances are described by the velocity gradients $\mathbf{L}_{I\_i} = \dot{\mathbf{F}}_{I\_i}\mathbf{F}^{-1}_{I\_i}$ and $\mathbf{L}_N = \dot{\mathbf{F}}_N\mathbf{F}^{-1}_N$:

$$\mathbf{L}_{I\_i} = \underbrace{\dot{\mathbf{F}}^e_{I\_i}\mathbf{F}^{e^{-1}}_{I\_i}}_{\mathbf{L}^e_{I\_i}} + \underbrace{\mathbf{F}^e_{I\_i}\dot{\mathbf{F}}^p_{I\_i}\mathbf{F}^{p^{-1}}_{I\_i}\mathbf{F}^{e^{-1}}_{I\_i}}_{\mathbf{L}^p_{I\_i}} \quad \text{and} \quad \mathbf{L}_N = \underbrace{\dot{\mathbf{F}}^e_N\mathbf{F}^{e^{-1}}_N}_{\mathbf{L}^e_N} + \underbrace{\mathbf{F}^e_N\dot{\mathbf{F}}^p_N\mathbf{F}^{p^{-1}}_N\mathbf{F}^{e^{-1}}_N}_{\mathbf{L}^p_N} \tag{3}$$

The velocity gradients $\mathbf{L}_{I\_i} = \mathbf{L}^e_{I\_i} + \mathbf{L}^p_{I\_i}$ and $\mathbf{L}_N = \mathbf{L}^e_N + \mathbf{L}^p_N$ are additively spit into elastic and inelastic velocity gradients. The inelastic velocity gradients $\mathbf{L}^p_{I\_i}$ and $\mathbf{L}^p_N$ may be written as:

$$\begin{aligned} \mathbf{L}^p_{I\_i} &= \mathbf{F}^e_{I\_i}\dot{\mathbf{F}}^p_{I\_i}\mathbf{F}^{p^{-1}}_{I\_i}\mathbf{F}^{e^{-1}}_{I\_i} = \mathbf{D}^p_{I\_i} + \mathbf{W}^p_{I\_i} \quad \text{and} \\ \mathbf{L}^p_N &= \mathbf{F}^e_N\dot{\mathbf{F}}^p_N\mathbf{F}^{p^{-1}}_N\mathbf{F}^{e^{-1}}_N = \mathbf{D}^p_N + \mathbf{W}^p_N \end{aligned} \tag{4}$$

where $\mathbf{D}^p_{I\_i}$ and $\mathbf{D}^p_N$ are the inelastic deformation rates (symmetric parts) and, $\mathbf{W}^p_{I\_i}$ and $\mathbf{W}^p_N$ are the inelastic spin rates (skew symmetric parts).

With no loss in generality, the inelastic flow is assumed irrotational [54], i.e. $\mathbf{W}^p_{I\_i} = \mathbf{W}^p_N = \mathbf{0}$, and the relations (4) give the evolution equations of the inelastic deformation gradients:

$$\dot{\mathbf{F}}^p_{I\_i} = \mathbf{F}^{e^{-1}}_{I\_i}\mathbf{D}^p_{I\_i}\mathbf{F}^e_{I\_i}\mathbf{F}^p_{I\_i} \quad \text{and} \quad \dot{\mathbf{F}}^p_N = \mathbf{F}^{e^{-1}}_N\mathbf{D}^p_N\mathbf{F}^e_N\mathbf{F}^p_N \tag{5}$$

in which the inelastic deformation rates $\mathbf{D}^p_{I\_i}$ and $\mathbf{D}^p_N$ take the following general forms:

$$\mathbf{D}^p_{I\_i} = \dot{\gamma}^p_{I\_i}\frac{\mathbf{T}'_{I\_i}}{\sqrt{2}\tau_{I\_i}} \quad \text{and} \quad \mathbf{D}^p_N = \dot{\gamma}^p_N\frac{\mathbf{T}'_N}{\sqrt{2}\tau_N} \tag{6}$$

where $\tau_{I\_i} = \left(\text{tr}\left(\mathbf{T}'_{I\_i}\mathbf{T}'^T_{I\_i}\right)\Big/2\right)^{1/2}$ and $\tau_N = \left(\text{tr}\left(\mathbf{T}'_N\mathbf{T}'^T_N\right)/2\right)^{1/2}$ are the effective shear stresses, $\mathbf{T}'_{I\_i} = \mathbf{T}_{I\_i} - \text{tr}\left(\mathbf{T}_{I\_i}\right)/3\mathbf{I}$ and $\mathbf{T}'_N = \mathbf{T}_N - \text{tr}\left(\mathbf{T}_N\right)/3\mathbf{I}$ are the deviators of the Cauchy stress tensors in which $\mathbf{I}$ is the unit tensor and, $\dot{\gamma}^p_{I\_i}$ and $\dot{\gamma}^p_N$ are the accumulated viscous strain rates constitutively specified in Section 2.3.

2.2. Stress decomposition

The strain-induced phase transformation characterizes the heterogeneity of the initially amorphous medium which may be treated in a composite framework considering a three-phase representation of the PLA microstructure, involving amorphous, mesomorphic and crystalline phases in the most general case. The progressive evolution of the remaining amorphous portion χ_a can be expressed using the volume fraction concept:

$$\chi_a = 1 - \chi_m - \chi_c \tag{7}$$

where χ_m and χ_c are the degrees of mesomorphic and crystalline phases, respectively, given by:

$$\chi_i = \phi_{\infty\_i}\kappa_i \tag{8}$$

in which ϕ_{∞_i} is the maximum degree of the newly formed phase and κ_i is the total degree of transformation.

The PLA material is thus considered as a mixture of mesomorphic, crystalline and amorphous phases in the most general case and the effective contribution of the three phases to the intermolecular Cauchy stress $\mathbf{T}_I$ is determined using a simple rule of mixture:

$$\mathbf{T}_I = \chi_a\mathbf{T}_{I\_a} + \chi_m\mathbf{T}_{I\_m} + \chi_c\mathbf{T}_{I\_c} \tag{9}$$

In such an approach, the phase amount is explicitly introduced in the model formulation. The three phases are however assumed to behave independently and without interaction. Although a more complex composite-type formulation could be used to capture the underlying interactions as well as the structure-response relationship [55,56], our goal is to propose a simple approach to describe in a unified manner the relationship between mesomorphic/crystalline phases and stress–strain response across the glass transition.

Although the phases resulting from quiescent melt [57] are different in morphology and in size than the newly formed phases due to

straining, their rates of transformation, $\dot{\kappa}_m$ and $\dot{\kappa}_c$, follow the classical phenomenological formula initially proposed by Avrami [58–60], for spherulitic growth in thermally-induced crystallization, and modified by Doufas et al. [61]:

$$\dot{\kappa}_i = \frac{\dot{\varepsilon}}{\dot{\varepsilon}_{ref}} m_i K_{av\_i} \left(-\ln\left(1-\kappa_i\right)\right)^{\frac{m_i-1}{m_i}} \left(1-\kappa_i\right) \tag{10}$$

where m_i is the Avrami exponent and K_{av_i} is the transformation rate function. The strain rate effect in Eq. (10) was introduced by Ahzi et al. [21] with $\dot{\varepsilon}$ the strain rate and $\dot{\varepsilon}_{ref}$ the reference strain rate taken equal to 0.01 /s in our simulations.

For the transformation rate function K_{av_i}, we adopt the general empirical form for PET, defined as follows:

$$K_{av\_i} = 1.47\times10^{-3}\left(\frac{4\pi N u_i}{3\phi_{\infty\_i}}\right)^{1/3} \exp\left(-\left(\frac{\theta-141}{47.33}\right)^2\right) \tag{11}$$

in which Nu_i is the number density of nuclei originally present in the amorphous phase.

It worth noticing that the Avrami formula may not be an adequate choice for the phase transformation in PLA and an improved evolution law could be provided from a thermodynamic reasoning [48]. Nonetheless, the Avrami formula may be regarded as a phenomenological description of the evolution of the two newly formed phases needed in the constitutive formulation.

The total Cauchy stress $\mathbf{T}$ in the polymer is given by:

$$\mathbf{T} = \mathbf{T}_I + \mathbf{T}_N \tag{12}$$

in which $\mathbf{T}_N$ is the molecular network Cauchy stress.

2.3. Constitutive equations

The two following subsections describe the constitutive theory for the intermolecular and network resistances.

2.3.1. Intermolecular

The intermolecular resistance produces the initial stiff response due to the intermolecular barriers (represented by the linear spring), followed by the intermolecular flow (represented by the viscous dashpot) characterized by the rate and temperature dependence of the yield. The three phases do not co-exist during the first steps of the loading due to the occurrence of the phase transformation at large strains. The elastic–viscoplastic region of the stress–strain curve is thus solely governed by the amorphous chains, in the glassy state or in the rubbery state according to the stretching temperature. The mesomorphic and crystalline intermolecular properties impact only the strain-hardening region of the stress–strain curve.

The amorphous, mesomorphic and crystalline intermolecular Cauchy stresses, $\mathbf{T}_{I\_a}$, $\mathbf{T}_{I\_m}$ and $\mathbf{T}_{I\_c}$, are constitutively related to the corresponding elastic deformation by the following law for linear elastic springs:

$$\mathbf{T}_{I\_i} = \frac{1}{J^e_{I\_i}} \mathbf{C}^e_{I\_i} \ln\left(\mathbf{V}^e_{I\_i}\right) \tag{13}$$

where $J^e_{I\_i} = \det \mathbf{F}^e_{I\_i}$ is the elastic volume change, $\ln\left(\mathbf{V}^e_{I\_i}\right)$ is the Hencky elastic strain and $\mathbf{C}^e_{I\_i}$ is the fourth-order elastic stiffness tensor of the amorphous, mesomorphic and crystalline phases. The three phases are assumed to be isotropic and the elastic stiffness tensor $\mathbf{C}^e_{I\_i}$ is simply given, in Cartesian components, by the following standard formulation:

$$\left(\mathbf{C}^e_{I\_i}\right)_{ijkl} = \frac{E_i}{2(1+\nu_i)}\left(\left(\delta_{ik}\delta_{jl}+\delta_{il}\delta_{jk}\right)+\frac{2\nu_i}{1-2\nu_i}\delta_{ij}\delta_{kl}\right) \tag{14}$$

in which δ_{ij} is the Kronecker-delta symbol, E_i and ν_i are the Young's modulus and the Poisson's ratio, respectively.

It is well known that important changes occur in the amorphous chain mobility around the glass transition temperature T_g leading to important stiffness variation with the temperature. The function given by Dupaix and Boyce [27] is used to model the dependence on temperature θ of the amorphous Young's modulus E_a below and above T_g:

$$E_a(\theta) = E_{g1} - E_{g2}\theta \quad \text{for} \quad \theta < T_g - \Delta T_g/2 \tag{15}$$

and

$$E_a(\theta) = \frac{1}{2}\left(E_{gr}-E_{r1}\right) - \frac{1}{2}\left(E_{gr}-E_{r1}\right)\tanh\left(\frac{5}{\Delta T_g}\left(\theta-T_g\right)\right) - E_{r2}\left(\theta-T_g\right) \quad \text{for} \quad \theta \geq T_g - \Delta T_g/2 \tag{16}$$

where ΔT_g is the interval of the temperature range across which the glass transition occurs, $E_{gr} = E_{g1} - E_{g2}\left(T_g - \Delta T_g/2\right)$ is the slope of the glassy region, E_{r1} is the slope of the rubbery region and E_{r2} is the slope of the linear drop across the glass transition region.

We assume that the inelastic flow in PLA is due to overcoming intermolecular resistances in both the amorphous phase and the two newly formed phases. The rate of viscous flow of each dashpot element follows an Arhenius-type expression for the thermally activated processes [19]:

$$\dot{\gamma}^p_{I\_i} = \gamma_{0\_i} \exp\left(-\frac{\Delta G_i}{k\theta}\left(1-\frac{\tau_{I\_i}}{s_i}\right)\right) \tag{17}$$

in which γ_{0_i} is the reference shear rate, k is the Boltzmann's constant, ΔG_i is the activation energy which must be overcome for flow to begin in phase i, s_i is an internal variable related to the resistance to shearing of the phase i. Both activation energy and shear strength are physically interpretable material constants capturing barrier to molecular chain segment rotation in the amorphous phase and barrier to shear in the two newly formed phases.

The strain-softening phenomenon occurring due to strain-induced disordering of the amorphous segments below T_g is simulated using the following evolution law:

$$\dot{s}_a = h\left(s_s - s_a\right)\dot{\gamma}^p_{I\_a} \tag{18}$$

where h is the slope of the yield drop with respect to strain, s_s is the steady-state value for s_a while its initial value is noted s_0.

2.3.2. Network

The network resistance produces two competitive processes: the molecular network stretching and orientation process (represented by the nonlinear spring) leading to the stress increase with deformation, and the thermal-induced molecular relaxation process (represented by the viscous dashpot) leading to the stress decrease by accommodating a part of the imposed deformation. The molecular network Cauchy stress $\mathbf{T}_N$ is expressed by the Arruda and Boyce statistically-based relationship [62]:

$$\mathbf{T}_N = \frac{1}{J^e_N}\frac{C_r}{3}\frac{\sqrt{N_{rl}}}{\overline{\lambda}^e_N}\mathrm{L}^{-1}\left(\frac{\overline{\lambda}^e_N}{\sqrt{N_{rl}}}\right)\left(\frac{1}{J^{e\,2/3}_N}\mathbf{F}^e_N\mathbf{F}^{e^T}_N - \overline{\lambda}^{e^2}_N\mathbf{I}\right) \tag{19}$$

in which $J^e_N = \det \mathbf{F}^e_N$ is the network volume change, C_r is the rubbery modulus, N_{rl} is the average number of rigid links in the chain (i.e. average chain length), $\mathrm{L}^{-1}(x) \approx x\left(3-x^2\right)/\left(1-x^2\right)$ is the inverse Langevin function approximated by a Padé approximant and $\overline{\lambda}^e_N = \left(\mathrm{tr}\left(J^{e^{-2/3}}_N \mathbf{F}^e_N\mathbf{F}^{e^T}_N\right)/3\right)^{1/2}$ is the stretch on each chain in the network. Note that the tensor $\mathbf{T}_N$ is deviatoric, i.e. $\mathbf{T}'_N = \mathbf{T}_N$. The material constants C_r and N_{rl} can be defined respectively by the slope of the stress–strain response at the strain-hardening and the strain at which the stress increases rapidly.

The rate of relaxation process $\dot{\gamma}^p_N$ is given by [19]:

$$\dot{\gamma}^p_N = C\left(\frac{1}{\lambda^p_N - 1}\right)\tau_N \tag{20}$$

where C is a viscous coefficient defining the temperature dependence of the relaxation and $\lambda^p_N = \left(\mathrm{tr}\left(\mathbf{F}^p_N\mathbf{F}^{p^T}_N\right)/3\right)^{1/2}$ for which the initial value is set slightly higher than one in order to avoid singularity of Eq. (20) and instability in the computations.

3. Experimentally-based material kinetics and parameter identification

The previous constitutive model is implemented into MATLAB software to simulate homogeneous deformation in PLA along with the microstructure evolution with strain. The model results will be compared to the database of Stoclet et al. [7,8,63]. The authors reported the large strain deformation response and the strain-induced phase transformation obtained by means of X-ray diffraction technique in an initially amorphous PLA, poly(D, L-lactide), purchased from Natureworks (USA) with a D-isomer fraction of 4.3%.

3.1. Presentation of the database

The experimental database is provided as symbols in Fig. 3 in which the material was strained under two strain rates (0.01 /s and 0.04 /s) over a wide range of temperatures below and above $T_g \sim 58$ °C. The stress–strain response of investigated PLA is provided in terms of true axial stress plotted vs. true axial strain. While the stress–strain curves at 0.04 /s are well available in the papers of Stoclet et al. [7,8], those at 0.01 /s are only available in the thesis manuscript of Stoclet [63]. A global view at Fig. 3 shows a strong dependence of strain rate, temperature and strain. Small temperature and strain rate changes result in significant changes of the material response along with the phase transformation. The schematic visualization given in the form of phase diagram in Fig. 1 highlights the complex phenomenon to be modeled.

For a strain rate of 0.01 /s and at a temperature of 45 °C, PLA is able to transform only in mesomorphic form. This is also true for higher temperatures but for a temperature of 70 °C, both oriented crystals and imperfect ordered mesomorphic forms co-exist in PLA. For a temperature of 75 °C, solely crystalline ordering is formed in PLA. A significant rate-dependency of the temperature effect on the strain-induced ordering has been observed. Indeed, whereas both crystalline and mesomorphic phases co-exist in PLA at 70 °C when the material is stretched at 0.01 /s, this co-existence is shifted to 80 °C when the strain rate is of 0.04 /s. From a certain temperature, neither the mesomorphic phase nor the crystalline phase develops. The mechanical behavior of PLA is highly nonlinear with the expected dependencies of the straining temperature on the different features of the stress–strain curves, especially, on the initial stiffness and the strain-hardening. Above the ductile/brittle transition temperature, located around 35 °C–45 °C, and below T_g the material exhibits the ductile response characteristic of glassy polymers with a strain-softening phenomenon after yield prior to the strain-hardening stage. Due to the increase in molecular mobility and chain orientation process the material behaves as a rubber-like material above T_g characterized by a relatively compliant response which stiffens with increasing strain.

The experiments in Fig. 3 constitute a fruitful database for the identification of the constitutive model for which several inputs are required:

- Phase transformation kinetics: ϕ_{∞_m}, ϕ_{∞_c}, Nu_m, Nu_c, m_m and m_c.
- Intermolecular parameters of the amorphous phase: E_{g1}, E_{g2}, E_{r1}, E_{r2}, γ_{0_a}, ΔG_a and s_0 (h and s_s if a strain-softening is present).
- Intermolecular parameters of the mesomorphic phase: E_m, γ_{0_m}, ΔG_m and s_m.
- Intermolecular parameters of the crystalline phase: E_c, γ_{0_c}, ΔG_c and s_c.
- Network parameters: C_r, N_{rl} and C.

As revealed by these experiments, the mesomorphic and crystalline phases are two relative mechanisms dependent on the straining temperature and the strain rate. The identification exercise is complex since a small variation of these loading conditions has a strong impact on their occurrence. Our goal is to propose a unified approach able to reproduce the microstructure evolution in PLA across the glass transition along with its elastic–viscoplastic–viscohyperelastic response.

In what follows, the identification scheme is divided into three separate and distinct steps: (i) We firstly design the phase transformation kinetics, (ii) then we determine the intermolecular response of the amorphous phase, and (iii) finally, by analyzing the strain-hardening part, we deduce the intermolecular response of the two newly formed phases and the network parameters.

3.2. Dual-phase transformation kinetics

The mechanism of phase transformation initiates beyond some critical strain. This strain of initiation is significantly influenced by the stretching temperature as shown in Fig. 4a, and is higher for crystalline phase than mesomorphic phase. Due to the detrimental effect of molecular relaxation on the molecular orientation necessary to form the mesomorphic/crystalline phases at a higher straining temperature, the initiation strain shifts to a higher value with increasing straining temperature. A linear relationship exists between the initiation strain and the straining temperature. It is well described for the mesomorphic and crystalline phases, respectively, by:

$$\varepsilon_{init\_m} = 0.013\theta - 0.117 \tag{21}$$

$$\varepsilon_{init\_c} = 0.01\theta + 0.225 \tag{22}$$

Similarly, the maximum degree of mesomorphic and crystalline phases is plotted in Fig. 4b as a function of temperature. While the strain of initiation appears to be relatively strain rate independent, an increase in strain rate shifts the maximum phase degree to higher temperatures.

The WLF time–temperature equivalence principle is used to superimpose the data by shifting them via a shift factor a_{θ_i} [64]:

$$\ln\left(a_{\theta\_i}\right) = \frac{C_{1\_i}\left(\theta - \theta_{ref}\right)}{C_{2\_i} + \theta - \theta_{ref}} \tag{23}$$

in which C_{1_i} and C_{2_i} are two adjustable parameters depending on the newly formed phase under consideration, and θ_{ref} is the reference temperature. Using a reference temperature θ_{ref} of 70 °C, $C_{1\_m} = 2$, $C_{2\_m} = 60$ °C, $C_{1\_c} = -5.47$ and $C_{2\_c} = 30$ °C, Fig. 5 presents the maximum degree of mesomorphic and crystalline phases as a function of the reduced strain rate $a_{\theta\_i}\dot{\varepsilon}$ such that a straight line fit perfectly describes the results. The simple linear relationships exhibit opposite slopes and are described for the respective phases by:

$$\phi_{\infty\_m} = 1.029 a_{\theta\_m}\dot{\varepsilon} + 0.121 \tag{24}$$

$$\phi_{\infty\_c} = -23.97 a_{\theta\_c}\dot{\varepsilon} + 0.4 \tag{25}$$

The opposite slopes in Fig. 5 are the sign of a complex competitive process with strong effects of temperature and strain rate. Both oriented crystals and imperfect ordered mesomorphic forms nucleate from a higher ordered structure than the amorphous phase that pre-exists in PLA [12,13]. We assume that the mesomorphic and crystalline phases originate from different nuclei. The number density of nuclei Nu_i is found dependent on the temperature as shown in Fig. 6 and described by two expressions for the mesomorphic and crystalline phases:

$$Nu_m = 8 \times 10^{10} \exp\left(-0.182\theta\right) \tag{26}$$

$$Nu_c = 1.1 \times 10^{9} \exp\left(-0.106\theta\right) \tag{27}$$

To complete the identification of the Avrami formula (10), the Avrami exponent is supposed to be the same for the two phases:

$$m_m = m_c = 2.0 \tag{28}$$

3.3. Stress–strain response

In what follows, we present the methodology for the parameter calibration with an interest on the whole available tensile deformation behavior.

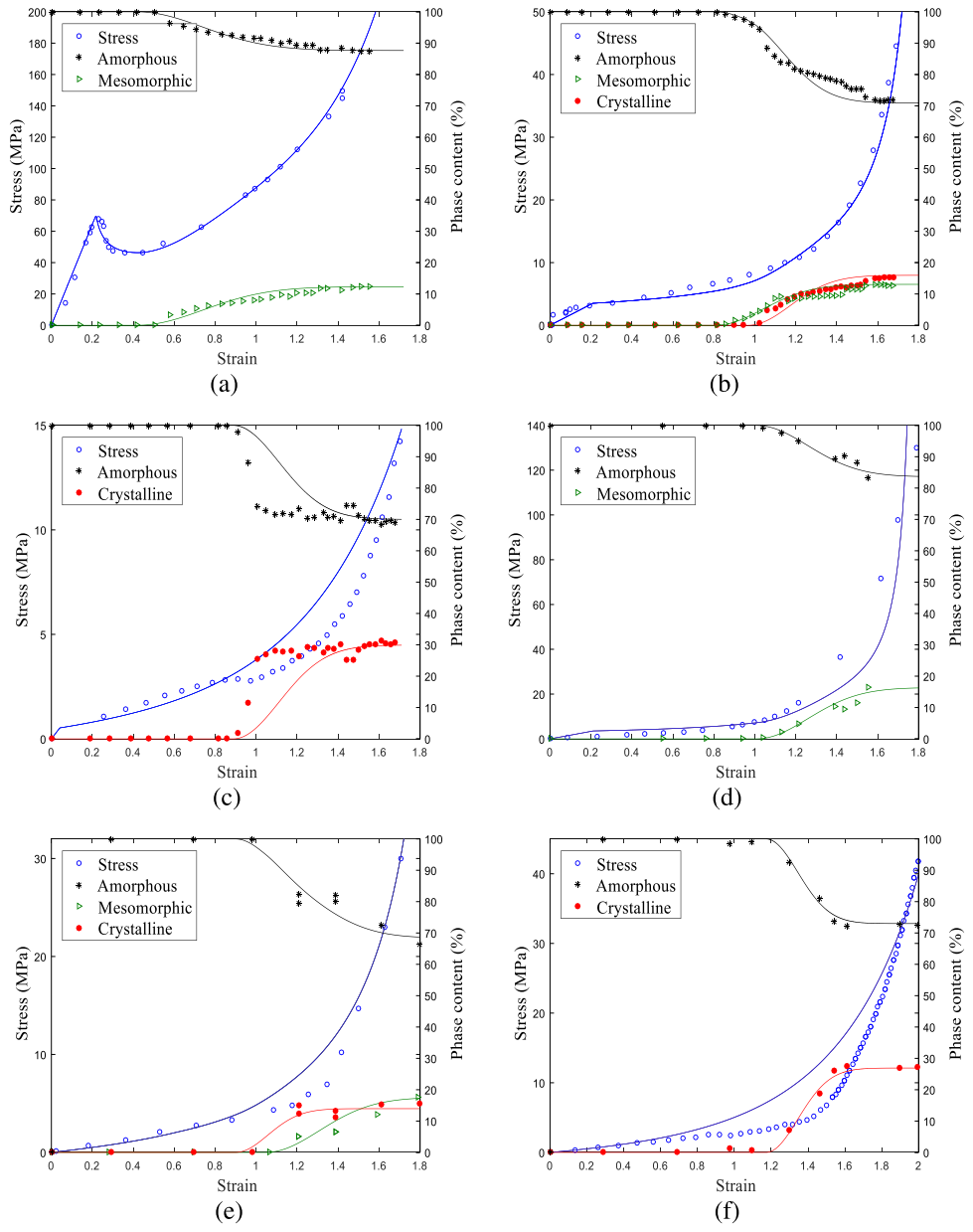

Fig. 3. Stress–strain response and material phase transformation (symbols: experiments [7,8,63], lines: model) at a strain rate $\dot{\epsilon}$ of 0.01 /s: (a) θ = 45 °C, (b) θ = 70 °C, (c) θ = 75 °C, and at a strain rate $\dot{\epsilon}$ of 0.04 /s: (d) θ = 70 °C, (e) θ = 80 °C, (f) θ = 90 °C.

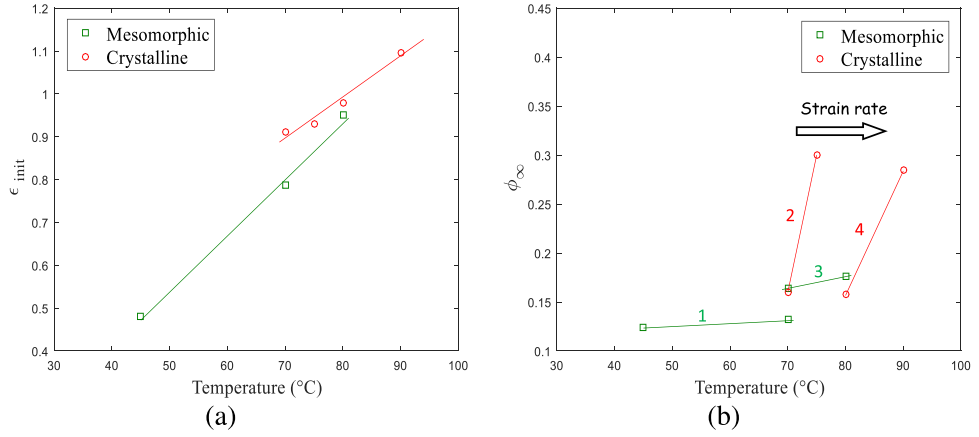

Fig. 4. Data extracted from Fig. 3 as a function of temperature: (a) strain of initiation (symbols: identified values, lines: Eqs. (21) and (22)), (b) maximum degree of mesomorphic and crystalline phases (1, 2: $\dot{\epsilon}$ = 0.01 /s, 3, 4: $\dot{\epsilon}$ = 0.04 /s).

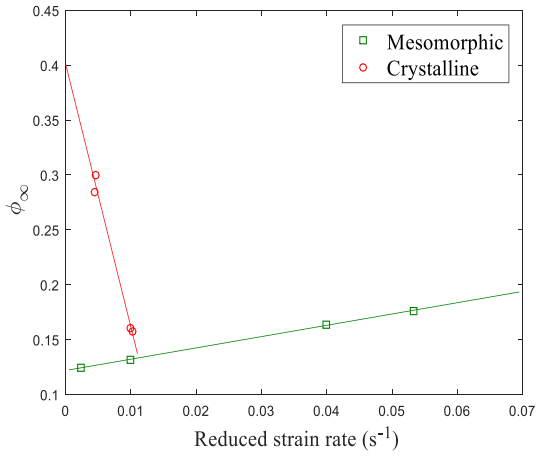

Fig. 5. Maximum degree of mesomorphic and crystalline phases as a function of reduced strain rate $a_{\theta\_i}\dot{\epsilon}$ (symbols: identified values, lines: Eqs. (24) and (25)).

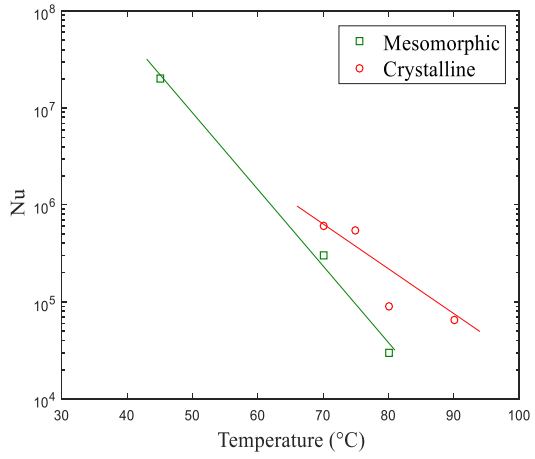

Fig. 6. Number density of nuclei as a function of temperature (symbols: identified values, lines: Eqs. (26) and (27)).

3.3.1. Intermolecular

The intermolecular resistance arises from a combination of amorphous, mesomorphic and crystalline stiffness and flow. The parameter calibration for the different phases is performed separately. With reference to the micromechanics concepts, we postulate that the properties of amorphous, mesomorphic and crystalline phases are the same whatever the phase content. By this way, the individual constitutive response of the three phases will be extracted.

3.3.1.1. Amorphous phase. The onset of phase transformation beginning after a strain of 40% (Fig. 4a) the intermolecular parameters of the amorphous phase, representative of its elastic–viscoplastic response, were determined using the initial part of the stress–strain curves. The elastic stiffness is reported in Fig. 7a as a function of temperature. It is constant over a wide range of temperatures in the glassy region, followed by a dramatic drop in the glass transition region and a more gradual decrease in the rubbery region. The fitting of the elastic stiffness–temperature data with the formulae (15) and (16) gives the following values for the involved parameters:

$$E_{g1} = 402.85 \text{ [MPa]} \tag{29}$$

$$E_{g2} = 2.273 \text{ [MPa]} \tag{30}$$

$$E_{r1} = 24.53 \text{ [MPa]} \tag{31}$$

$$E_{r2} = 0.783 \left[\text{MPa } ^\circ\text{C}^{-1}\right] \tag{32}$$

The amorphous yield properties, i.e. the material parameters involved in the Arhenius-type relation (17), were identified using the experimental yield strength. The amorphous value of the pre-exponential factor γ_{0_a} was fixed to a prescribed value:

$$\gamma_{0\_a} = 1.75 \times 10^6 \left[\text{s}^{-1}\right] \tag{33}$$

The other parameters in Eq. (17), ΔG_a and s_0, were successively iterated, by means of trial and error, in order to achieve optimal agreement between the simulations and the yield strength. The amorphous activation energy takes the following value:

$$\Delta G_a = 8 \times 10^{-19} \text{ [J]} \tag{34}$$

The resistance to shearing s_0 is given in Fig. 7b as a function of temperature and follows the following expression:

$$s_0 = 1.434 \times 10^4 \exp(-0.1307\theta) \text{ [MPa]} \tag{35}$$

The strain-softening phenomenon appearing at 45 °C is represented by the formula (18) with the following parameter values:

$$h = 140.0 \tag{36}$$

$$s_s = 21.0 \text{ [MPa]} \tag{37}$$

The strain-hardening response is dominated by the molecular orientation and relaxation, and the occurrence of strain-induced phases. The intermolecular parameters of crystalline and mesomorphic phases were

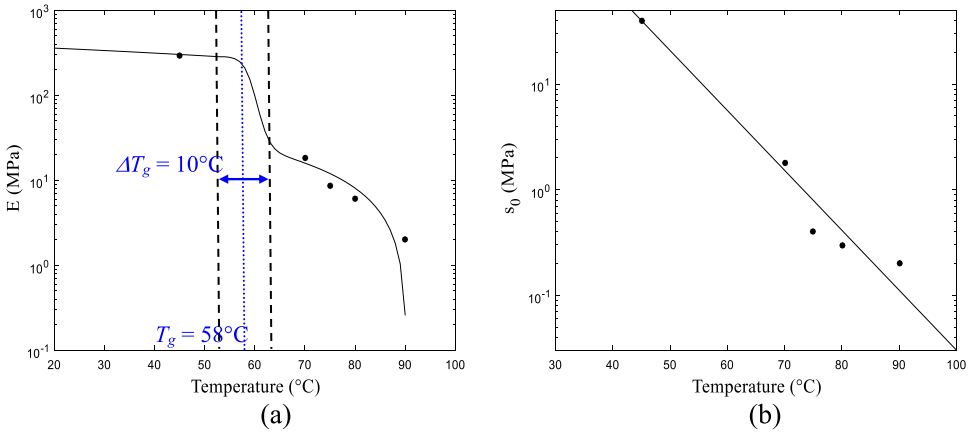

Fig. 7. Amorphous intermolecular parameters as a function of temperature: (a) Young's modulus (symbols: identified value, line: Eqs. (15) and (16)), (b) initial shear strength (symbols: identified values, line: Eq. (35)).

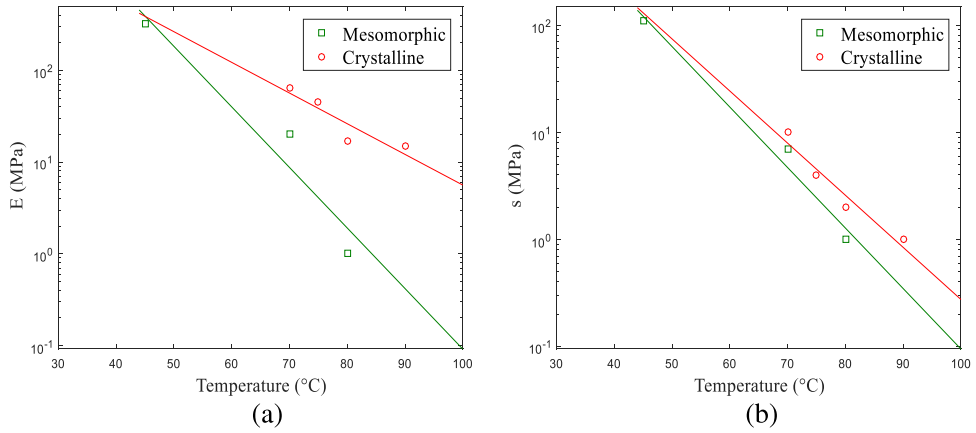

Fig. 8. Mesomorphic and crystalline intermolecular parameters as a function of temperature: (a) Young's modulus (symbols: identified values, lines: Eqs. (38) and (39)), (b) shear strength (symbols: identified values, lines: Eqs. (42) and (43)).

optimized to fit correctly the stress–strain data in the strain-hardening region, simultaneously with the network parameters.

3.3.1.2. Mesomorphic and crystalline phases. In order to ensure a realistic description of the microstructure a difference between the intermolecular parameter values of mesomorphic and crystalline phases is imposed. The mesomorphic and crystalline Young's moduli are plotted as a function of temperature in Fig. 8a and described by the following relations:

$$E_m = 365688\exp(-0.152\theta)\ \text{[MPa]} \tag{38}$$

$$E_c = 12411\exp(-0.077\theta)\ \text{[MPa]} \tag{39}$$

The mesomorphic and crystalline values of the pre-exponential factor are taken equal to the amorphous value, i.e. $\gamma_{0\_m} = \gamma_{0\_c} = \gamma_{0\_a}$. The activation energies of mesomorphic and crystalline phases take the following values:

$$\Delta G_m = 7.5\times10^{-19}\ \text{[J]} \tag{40}$$

$$\Delta G_c = 7\times10^{-19}\ \text{[J]} \tag{41}$$

The mesomorphic and crystalline resistances to shearing are plotted as a function of temperature in Fig. 8b and described by:

$$s_m = 41918\exp(-0.13\theta)\ \text{[MPa]} \tag{42}$$

$$s_c = 20095\exp(-0.112\theta)\ \text{[MPa]} \tag{43}$$

3.3.2. Network

Figs. 9 and 10a shows the calibration result of the network parameters as a function of temperature. As shown in Fig. 9a, the dependence on temperature of the parameter C_r follows a classical behavior on both sides of T_g, decreasing below T_g and increasing above T_g. The linear phenomenological model of Richeton et al. [29] is adopted to describe the behavior of the parameter C_r below and above T_g:

$$C_r = 47.07 - 0.8\theta\ \text{[MPa]}\ \text{ for } \theta \le T_g \tag{44}$$

and

$$C_r = \left(47.07 - 0.8T_g\right)\frac{\theta}{T_g}\ \text{[MPa]}\ \text{ for } \theta \ge T_g \tag{45}$$

The parameter C characterizes the thermal-induced chain relaxation process increasing linearly with increasing temperature but with different slopes on both sides of T_g as shown in Fig. 9b. The bi-linear evolution of the parameter C is independent on the appearing phase. That is to say that only the temperature dependence is introduced. A similar linear phenomenological model that for the parameter C_r is proposed for the behavior of the parameter C below and above T_g [32]:

$$C = 7.011\times10^{-7} + 2.2\times10^{-9}\theta\ \left[\text{MPa}^{-1}\ \text{s}^{-1}\right]\ \text{ for } \theta \le T_g \tag{46}$$

and

$$C = \left(7.011\times10^{-7} + 2.2\times10^{-9}T_g\right)\frac{\theta}{T_g}\ \left[\text{MPa}^{-1}\ \text{s}^{-1}\right]\ \text{ for } \theta \ge T_g \tag{47}$$

The identification exercise ends with the parameter N_{rl} controlling the orientation-induced strain-hardening. It is plotted as a function of temperature in Fig. 10a. If the occurrence of phases is distinguished, as illustrated in the figure, it can be seen that the parameter N_{rl} increases with increasing temperature below T_g and remains constant above T_g. This is consistent with the classical evolution of the parameter N_{rl} [29]. However, the change from the glassy to the rubbery state involves two distinct slopes. When the two strain-induced substructures coexist the slope is very low whereas it is very important when solely the crystallization occurs. That highlights the complexity of the two interacting processes, namely, the strain-induced orientation and the thermal-induced molecular relaxation, both governed by the straining temperature and the strain rate as discussed in the introduction using the diagram in Fig. 1. The important molecular relaxation at high straining temperature, translated by the parameter C in Fig. 9b, imposes higher values of the parameter N_{rl} due to the solely occurrence of the crystallization. When the latter is accompanied by the mesomorphic phase, smaller values of the parameter N_{rl} are necessary. Therefore, the parameter N_{rl} may be also related to the amount of crystalline phase. Keeping in mind that the transformed PLA material is seen as a composite, the parameter N_{rl} is plotted as a function of amount of the non-crystalline portion in Fig. 10b. This plotting allows formulating a simple exponential function:

$$N_{rl} = 11.72 + 64\times10^4\exp\left(-14.21\left(1-\phi_{\infty\_c}\right)\right) \tag{48}$$

in which ϕ_{∞_c} is given by Eq. (25) as a function of the reduced strain rate $a_{\theta\_c}\dot{\varepsilon}$.

3.4. Comparison between experiments and model

Fig. 3 presents the comparison of model simulations with experimental stress–strain curves and phase changes. The lines represent the simulation results while the symbols designate the experimental data. A global view at these results shows that the general trends provided by the model are satisfactory for the different straining temperatures including the rate-dependency. The model provides a good description of the microstructure evolution with strain and the main features of the stress–strain curve across the glass transition: the initial elastic response, the yield event (if any) followed by the steady state flow, the strain-hardening and the dramatic strain-hardening at very large strains.

The results reported in Fig. 3 illustrate the dependence of various features of the stress–strain curve on straining temperature and strain

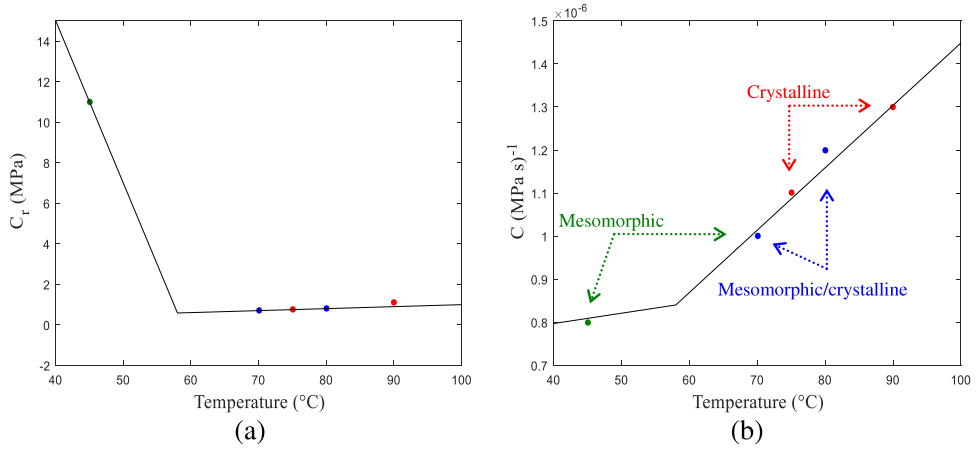

Fig. 9. Rubbery modulus and viscous coefficient as a function of temperature: (a) rubbery modulus (symbols: identified values, lines: Eqs. (44) and (45)), (b) viscous coefficient (symbols: identified values, lines: Eqs. (46) and (47)).

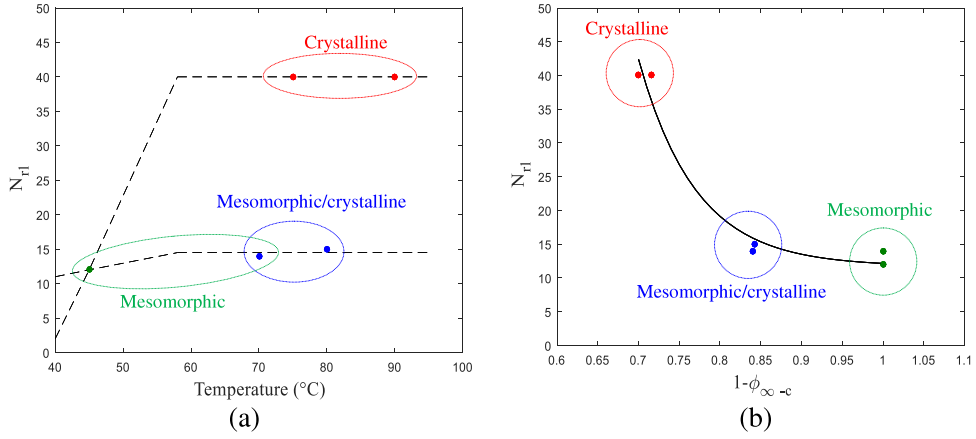

Fig. 10. Average chain length as a function of: (a) temperature and (b) amount of the non-crystalline portion (symbols: identified values, line: Eq. (48)).

rate. However, the microstructure effect on the mechanical response cannot be assessed. We can use the proposed model to discuss the benefits or prejudices of the mechanism of phase changes on the material response.

3.5. Implication of the phase changes

Let us first show how the kinetics of phase transformation modifies the large-strain mechanical behavior. To illustrate this important feature, we re-consider in Fig. 11, the results presented in Fig. 3 in which, respectively, only the mesomorphic phase (Fig. 3a), the two phases (Fig. 3b) and only the crystalline phase occur (Fig. 3f). Fig. 11 presents the different cases in which no phase change occurs and only one phase or both phases appear. The figure shows that the presence of phases affects strongly the strain-hardening region. The mesomorphic phase has a preponderant effect below T_g and a minor effect above T_g. More interestingly, the crystallization-induced softening, also reported in NR [48,50], is well accounted for by our approach.

As a final point of discussion, we propose to examine the model response under continuous relaxation. Stoclet et al. [8] measured the phase changes under continuous relaxation with jumps in temperature, and the data are reported in Fig. 12a. The test consisted firstly to apply a relaxation (i.e. $\dot{\epsilon}$ is zero) at a temperature of 45 °C for a prescribed delay during which the phase changes and the stress were measured. Secondly, a ramp in temperature to 65 °C and then to 70 °C were realized while the material is still under relaxation. The passage from one temperature to the other is carried out progressively as shown in the figure. While the strain-induced phase transformation in NR exhibits a time-dependent behavior during relaxation [48], the results of Fig. 12a show that the mechanism remains frozen in PLA. Fig. 12b presents the simulated curves according to the experimental protocol. Although some discrepancies can be observed, a general quite good agreement is obtained. Indeed, the model is able to capture the dependence on temperature of stress and occurrence of the two newly formed phases, both below and above T_g. The thermo-mechanical stability of the mesomorphic phase up to 70 °C is also a feature reproduced by the model.

4. Concluding remarks

In this work, we have presented a constitutive model for the PLA mechanical response across the glass transition in connection to strain-induced dual-phase transformation. The resistance to deformation in the PLA material is assumed to be the sum of a network part and an intermolecular part, the latter being a mixture of mesomorphic, crystalline and amorphous contributions. The properties of each phase were isolated using the experimental data of an initially amorphous PLA strained over a wide range of temperatures and two strain rates. The model was shown useful to understand the benefits or prejudices of each mechanism: Below the glass transition, the mesomorphic phase stiffens the strain-hardening. Above the glass transition, the mesomorphic phase is thermo-mechanically stable but has a minor effect on the material response compared to the crystalline phase which softens the strain-hardening.

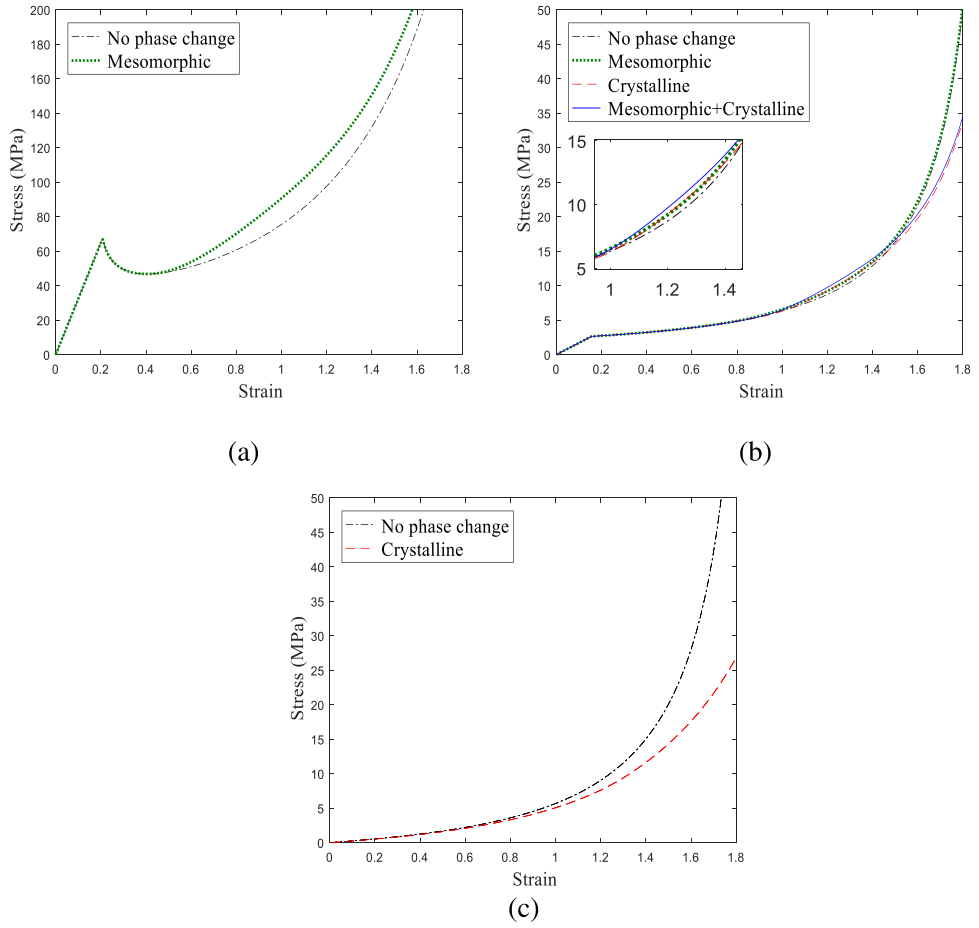

Fig. 11. Effect of phase transformation on the stress–strain curve: (a) $\dot{\varepsilon} = 0.01$ /s and $\theta = 45$ °C (corresponding to Fig. 3a), (b) $\dot{\varepsilon} = 0.01$ /s and $\theta = 70$ °C (Fig. 3b), (c) $\dot{\varepsilon} = 0.04$ /s and $\theta = 90$ °C (Fig. 3f).

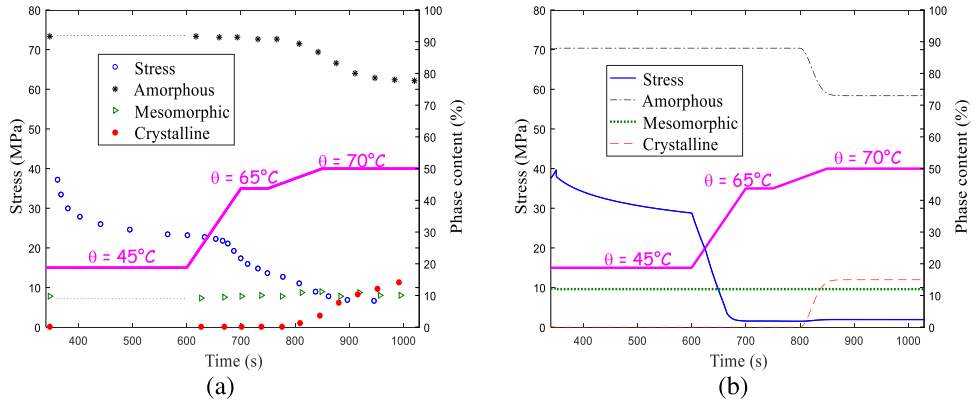

Fig. 12. Stress–time response and material phase transformation under continuous relaxation with jumps in temperature: (a) experiments from Stoclet et al. [8], (b) model simulation.

Our approach, although quite sophisticated and correctly reproducing the experimental observations, needs improvement for a fully realistic description of the microstructure evolution such as the deformation-induced anisotropy and the interactions between substructures. The verification of model capabilities under different mechanical loading paths is an important issue for further studies.

References

[1] D. Garlotta, A literature review of poly(lactic acid), J. Polymers Environ. 9 (2002) 63–84.
[2] R. Auras, B. Harte, S.E.M. Selke, An overview of polylactides as packaging materials, Macromol. Biosci. 4 (2004) 835–864.
[3] J. Mulligan, M. Cakmak, Nonlinear mechanooptical behavior of uniaxially stretched poly(lactic acid): dynamic phase behavior, Macromolecules 38 (2005) 2333–2344.

[4] R. Auras, L.T. Lim, S.E.M. Selke, H. Tsuji, Poly(Lactic Acid): Synthesis, Structures, Properties, Processing, and Applications, in: (Wiley Series on Polymer Engineering and Technology), John Wiley & Sons, 2010.
[5] S. Belbachir, F. Zaïri, G. Ayoub, U. Maschke, M. Naït-Abdelaziz, J.M. Gloaguen, M. Benguediab, J.M. Lefebvre, Modelling of photodegradation effect on elastic-viscoplastic behaviour of amorphous polylactic acid films, J. Mech. Phys. Solids 58 (2010) 241–255.
[6] R.E. Drumright, P.R. Gruber, D.E. Henton, Polylactic acid technology, Adv. Mater. 12 (2000) 1841–1846.
[7] G. Stoclet, R. Seguela, J.M. Lefebvre, S. Elkoun, C. Vanmansart, Strain-induced molecular ordering in polylactide upon uniaxial stretching, Macromolecules 43 (2010) 1488–1498.
[8] G. Stoclet, R. Seguela, J.M. Lefebvre, C. Rochas, New insights on the strain-induced mesophase of poly(d,l-lactide): in situ WAXS and DSC study of the thermo-mechanical stability, Macromolecules 43 (2010) 7228–7237.
[9] R. Lv, B. Na, N. Tian, S. Zou, Z. Li, S. Jiang, Mesophase formation and its thermal transition in the stretched glassy polylactide revealed by infrared spectroscopy, Polymer 52 (2011) 4979–4984.
[10] S. Saeidlou, M.A. Li, H. Huneault, C.B. Park, Poly(lactic acid) crystallization, Prog. Polym. Sci. 37 (2012) 1657–1677.
[11] Y. Wang, L. Liu, M. Li, W. Cao, C. Liu, Spectroscopic analysis of post drawing relaxation in poly(lactic acid) with oriented mesophase, Polymer Testing 43 (2015) 103–107.
[12] C. Zhou, H. Li, Y. Zhang, F. Xue, S. Huang, H. Wen, J. Li, J. de Claville Christiansen, D. Yu, Z. Wu, S. Jiang, Deformation and structure evolution of glassy poly(lactic acid) below the glass transition temperature, CrystEngComm 17 (2015) 5651–5663.
[13] C. Zhou, H. Guo, J. Li, S. Huang, H. Li, Y. Meng, D. Yu, J. de Claville Christiansen, S. Jiang, Temperature dependence of poly(lactic acid) mechanical properties, Roy. Soc. Chem. Adv. 6 (2016) 113762–113772.
[14] Z. Chen, S. Zhang, F. Wu, W. Yang, Z. Liu, M. Yan, Motion mode of poly(lacticacid) chains in film during strain-induced crystallization, J. Appl. Polym. Sci. 133 (2016) 42969.
[15] S. Farah, D.G. Anderson, R. Langer, Physical and mechanical properties of PLA, and their functions in widespread applications - a comprehensive review, Adv. Drug Deliv. Rev. 107 (2016) 367–392.
[16] K. Masutani, Y. Kimura, Present situation and future perspectives of poly(lactic acid), in: M.L. Di Lorenzo, R. Androsch (Eds.), Synthesis, Structure and Properties of Poly(Lactic Acid), 2017, pp. 1–25.
[17] C.P. Buckley, D.C. Jones, Glass-rubber constitutive model for amorphous polymers near the glass transition, Polymer 36 (1995) 3301–3312.
[18] A.M. Adams, C.P. Buckley, D.P. Jones, Biaxial hot drawing of poly(ethylene terephthalate): measurements and modelling of strain-stiffening, Polymer 41 (2000) 771–786.
[19] M.C. Boyce, S. Socrate, P.G. Llana, Constitutive model for the finite deformation stress–strain behavior of poly(ethylene terephthalate) above the glass transition, Polymer 41 (2000) 2183–2201.
[20] I.J. Rao, K.R. Rajagopal, A study of strain-induced crystallization of polymers, Int. J. Solids Struct. 38 (2001) 1149–1167.
[21] S. Ahzi, A. Makradi, R.V. Gregory, D.D. Edie, Modeling of deformation behavior and strain-induced crystallization in poly(ethylene terephthalate) above the glass transition temperature, Mech. Mater. 35 (2003) 1139–1148.
[22] I.J. Rao, Effect of the rate of deformation on the crystallization behavior of polymers, Int. J. Non-Linear Mech. 38 (2003) 663–676.
[23] A. Makradi, S. Ahzi, R.V. Gregory, D.D. Edie, A two-phase self-consistent model for the deformation and phase transformation behavior of polymers above the glass transition temperature: application to PET, Int. J. Plast. 21 (2005) 741–758.
[24] F. Zaïri, K. Woznica, M. Naït-Abdelaziz, Phenomenological nonlinear modelling of glassy polymers, C. R. Mec. 333 (2005) 359–364.
[25] R.B. Dupaix, D. Krishnan, A constitutive model for strain-induced crystallization in poly(ethylene terephthalate) (PET) during finite strain load-hold simulations, J. Eng. Mater. Technol. 128 (2006) 28–33.
[26] J.E. Shepherd, D.L. McDowell, K.I. Jacob, Modeling morphology evolution and mechanical behavior during thermo-mechanical processing of semi-crystalline polymers, J. Mech. Phys. Solids 54 (2006) 467–489.
[27] R.B. Dupaix, M.C. Boyce, Constitutive modeling of the finite strain behavior of amorphous polymers in and above the glass transition, Mech. Mater. 39 (2007) 39–52.
[28] M. Pyrz, F. Zaïri, Identification of viscoplastic parameters of phenomenological constitutive equations for polymers by deterministic and evolutionary approach, Model. Simul. Mater. Sci. Eng. 15 (2007) 85–103.
[29] J. Richeton, S. Ahzi, K.S. Vecchio, F.C. Jiang, A. Makradi, Modeling and validation of the large deformation inelastic response of amorphous polymers over a wide range of temperatures and strain rates, Int. J. Solids Struct. 44 (2007) 7938–7954.
[30] F. Zaïri, M. Naït-Abdelaziz, J.M. Gloaguen, J.M. Lefebvre, Modelling of the elasto-viscoplastic damage behaviour of glassy polymers, Int. J. Plast. 24 (2008) 945–965.
[31] C. Regrain, L. Laiarinandrasana, S. Toillon, K. Saï, Multi-mechanism models for semi-crystalline polymer: constitutive relations and finite element implementation, Int. J. Plast. 25 (2009) 1253–1279.
[32] G. Ayoub, F. Zaïri, M. Naït-Abdelaziz, J.M. Gloaguen, Modelling large deformation behaviour under loading-unloading of semicrystalline polymers: application to a high density polyethylene, Int. J. Plast. 26 (2010) 329–347.
[33] F. Zaïri, M. Naït-Abdelaziz, J.M. Gloaguen, J.M. Lefebvre, Constitutive modelling of the large inelastic deformation behaviour of rubber-toughened poly(methyl methacrylate): effects of strain rate, temperature and rubber-phase volume fraction, Model. Simul. Mater. Sci. Eng. 18 (2010) 1–22.
[34] G. Ayoub, F. Zaïri, C. Fréderix, J.M. Gloaguen, M. Naït-Abdelaziz, R. Seguela, J.M. Lefebvre, Effects of crystal content on the mechanical behaviour of polyethylene under finite strains: experiments and constitutive modelling, Int. J. Plast. 27 (2011) 492–511.
[35] F. Zaïri, M. Naït-Abdelaziz, J.M. Gloaguen, J.M. Lefebvre, A physically-based constitutive model for anisotropic damage in rubber-toughened glassy polymers during finite deformation, Int. J. Plast. 27 (2011) 25–51.
[36] L. Chevalier, Y.M. Luo, E. Monteiro, G.H. Menary, On visco-elastic modelling of polyethylene terephthalate behaviour during multiaxial elongations slightly over the glass transition temperature, Mech. Mater. 52 (2012) 103–116.
[37] M. Poluektov, J.A.W. van Dommelen, L.E. Govaert, I. Yakimets, M.G.D. Geers, Micromechanical modelling of short-term and long-term large-strain behaviour of polyethylene terephthalate, Model. Simul. Mater. Sci. Eng. 21 (2013) 085015.
[38] H. Abdul-Hameed, T. Messager, F. Zaïri, M. Naït-Abdelaziz, Large-strain viscoelastic-viscoplastic constitutive modeling of semi-crystalline polymers and model identification by deterministic/evolutionary approach, Comput. Mater. Sci. 90 (2014) 241–252.
[39] F. Gehring, J.L. Bouvard, N. Billon, Modeling of time dependent mechanical behavior of polymers: comparison between amorphous and semicrystalline polyethylene terephthalate, J. Appl. Polym. Sci. 133 (2016) 43837–43854.
[40] R. Xiao, H. Sun, W. Chen, A finite deformation fractional viscoplastic model for the glass transition behavior of amorphous polymers, Int. J. Non-Linear Mech. 93 (2017) 7–14.
[41] J.R. Katz, Rontgenspektrographische untersuchungen am gedehnten kautschuk und ihre mogliche bedeutung fur das problem der dehnungseigenschaften dieser substanz, Naturwissenschaften 13 (1925) 410–416.
[42] P.J. Flory, Thermodynamics of crystallization in high polymers, I. Crystallization induced by stretching, J. Chem. Phys. 15 (1947) 397–408.
[43] M. Kroon, A constitutive model for strain-crystallising rubber-like materials, Mech. Mater. 42 (2010) 873–885.
[44] R. Dargazany, V.N. Khiem, E.A. Poshtan, M. Itskov, Constitutive modeling of strain-induced crystallization in filled rubbers, Phys. Rev. E 89 (2014) 022604.
[45] S.J. Mistry, S. Govindjee, A micro-mechanically based continuum model for strain-induced crystallization in natural rubber, Int. J. Solids Struct. 51 (2014) 530–539.
[46] J. Guilie, L. Thien-Nga, P. Le Tallec, Micro-sphere model for strain-induced crystallisation and three-dimensional applications, J. Mech. Phys. Solids 81 (2015) 58–74.
[47] R. Rastak, C. Linder, A non-affine micro-macro approach to strain-crystallizing rubber-like materials, J. Mech. Phys. Solids 111 (2018) 67–99.
[48] Q. Guo, F. Zaïri, X. Guo, Thermodynamics and mechanics of stretch-induced crystallization in rubbers, Phys. Rev. E 97 (2018) 052501.
[49] A.D. Drozdov, Mechanically induced crystallization of polymers, Int. J. Non-Linear Mech. 34 (1999) 807–821.
[50] P.A. Albouy, P. Sotta, Strain-induced crystallization in natural rubber, Adv. Polymer Sci. 277 (2017) 167–205.
[51] S. Ran, Z. Wang, C. Burger, B. Chu, B.S. Hsiao, Mesophase as the precursor for strain-induced crystallization in amorphous poly(ethylene terephthalate) film, Macromolecules 35 (2002) 10102–10107.
[52] L.V. Todorov, C.I. Martins, J.C. Viana, Solid-state structural evolution of poly(ethylene terephthalate) during step uniaxial stretching from different initial morphologies: an in situ wide angle x-ray scattering study, J. Appl. Polym. Sci. 124 (2012) 470–483.
[53] E.H. Lee, Elastic–plastic deformation at finite strains, J. Appl. Mech. 36 (1969) 1–6.
[54] M.E. Gurtin, L. Anand, The decomposition F= Fe Fp material symmetry and plastic irrotationality for solids that are isotropic-viscoplastic or amorphous, Int. J. Plast. 21 (2005) 1686–1719.
[55] F. Zaïri, J.M. Gloaguen, M. Naït-Abdelaziz, A. Mesbah, J.M. Lefebvre, Study of the effect of size and clay structural parameters on the yield and post-yield response of polymer/clay nanocomposites via a multiscale micromechanical modelling, Acta Mater. 59 (2011) 3851–3863.
[56] K. Hachour, F. Zaïri, M. Naït-Abdelaziz, J.M. Gloaguen, M. Aberkane, J.M. Lefebvre, Experiments and modeling of high-crystalline polyethylene yielding under different stress states, Int. J. Plast. 54 (2014) 1–18.
[57] H. Yamane, K. Sasai, Effect of the addition of poly(d-lactic acid) on the thermal property of poly(l-lactic acid), Polymer 44 (2003) 2569–2575.
[58] M. Avrami, Kinetics of phase change. I. General theory, J. Chem. Phys. 7 (1939) 1103–1112.
[59] M. Avrami, Kinetics of phase change. II. Transformation-time relations for random distribution of nuclei, J. Chem. Phys. 8 (1940) 212–224.
[60] M. Avrami, Phase change microstructure. III. Kinetics of phase change, J. Chem. Phys. 9 (1941) 177–184.
[61] A.K. Doufas, A.J. McHugh, C. Miller, Simulation of melt spinning including flow-induced crystallization part I. Model development and predictions, J. Non-Newton. Fluid Mech. 92 (2000) 27–66.
[62] E.M. Arruda, M.C. Boyce, A three-dimensional constitutive model for the large stretch behavior of rubber elastic materials, J. Mech. Phys. Solids 41 (1993) 389–412.
[63] G. Stoclet, Etude de la Structuration à Différents Niveaux D'échelle et du Comportement Thermomécanique d'un Polymère Issu de Ressources Renouvelables: L'Acide Poly(Lactique), Ph.D. thesis, Lille University, 2009.
[64] M.L. Williams, R.F. Landel, J.D. Ferry, The temperature dependence of relaxation mechanisms in amorphous polymers and other glass-forming liquids, J. Am. Chem. Soc. 77 (1955) 3701–3707.